Available online at www.sciencedirect.com
ScienceDirect
Applied Energy 00 (2021) 1–25
Applied Energy

Frequency and Voltage Coordinated Control of a Grid of AC/DC Microgrids

Baheej Alghamdi[a], Claudio Cañizares[b,*]

[a] *Department of Electrical and Computer Engineering, King Abdulaziz University, Jeddah, Saudi Arabia*
[b] *Department of Electrical and Computer Engineering, University of Waterloo, Waterloo, ON, N2L 3G1, Canada*

Abstract

This paper proposes a hierarchical control scheme based on a distributed controller design for a multi-microgrid system. Thus, a proposed control approach of ac and dc microgrid interfaces is presented, based on virtual synchronous generators to control the power exchange of the interconnected microgrids, and provide frequency support, voltage regulation, and virtual inertia for the individual microgrids and ac host grid. A hierarchical distributed control technique is proposed, with primary controls of interfacing virtual synchronous generators providing adaptive inertia for all ac systems, while a secondary distributed control regulates the frequency and the voltages of the ac host grid and the interconnected ac and dc microgrids, based on a consensus technique with limited information about the overall system. The proposed controller shares the total system load among the grid and microgrids, while minimizing the overall frequency and dc-voltage deviations in all interconnected systems. The presented interface and the controller are implemented, tested, and validated using time-domain simulations for a multi-microgrid test system, which is based on a CIGRE benchmark medium voltage system and consists of both ac and dc microgrids.

© 2021 Published by Elsevier Ltd.

Keywords: AC/DC microgrids, active distribution networks, adaptive inertia, adaptive damping, distributed control, frequency and voltage control, virtual synchronous generator.

Abbreviations & Nomenclature

Acronyms

ADN	Active Distribution Network
B2B	Back-to-Back
BESS	Battery Energy Storage System
DER	Distributed Energy Resources
EMS	Energy Management System
MG	Microgrid
MMG	Multi-microgrid
PLL	Phase Locked Loop
PV	Photo Voltaic
SG	Synchronous Generator
VFC	Voltage Frequency Control
VSC	Voltage Source Converter
VSG	Virtual Synchronous Generator

☆This work was supported by King Abdulaziz University in Jeddah, Saudi Arabia and NSERC, Canada.
*Corresponding author
Email addresses: baaalgamdi@kau.edu.sa (Baheej Alghamdi), ccanizar@uwaterloo.ca (Claudio Cañizares)

WG Wind Generator

Indices

i, j Microgrid VSG interfaces

Parameters

α_{P_l} Active power load exponent

$\gamma_o^{'}$ Index value corresponding to the nominal frequency γ_o of the host grid

γ_{max} Maximum allowable frequency or dc voltage deviations

γ_{min} Minimum allowable frequency or dc voltage deviations

$\mathcal{E}$ Vector that represents the links from node v_i to node v_j

$\mathcal{V}$ Vector that contains vertices or nodes of the graph

$\overline{\Delta f}$ Maximum allowable frequency deviation (Hz)

τ_Q Output reactive power filter (s)

τ_{1_Q} VFC lead time constant (s)

$\tau_{1_{dc}}$ VSG adaptive damping lead time constant (s)

τ_{2_Q} VFC lag time constant (s)

$\tau_{2_{dc}}$ VSG adaptive damping lag time constant (s)

τ_{dc} VSG adaptive damping angular velocity filter (s)

τ_{gov} VSG Governor time constant (s)

A_G Connectivity matrix

a_{ij} Weights of connectivity matrix

b_i Pinning gain

C_f Inverter output filter capacitor (F)

C_{dc} DC DER output filter capacitor (F)

D_{ac} VSG Damping constant of ac MG interface (s)

D_{big} VSG damping coefficient during faults (s)

D_{dc} VSG Damping constant of dc MG interface (s)

D_o VSG nominal damping coefficient (s)

f_o Nominal frequency (Hz)

f_{max} Maximum allowable system frequency (Hz)

f_{min} Minimum allowable system frequency (Hz)

G Bidirectional communication graph

G_{ff} First-order transfer function of a feed-forward filter

J_{ac} Moment of Inertia of ac MG VSG interface (s^2)

J_{big} VSG moment of inertia constant during acceleration (s^2)

J_{dc} Moment of Inertia of dc VSG interface (s^2)

J_{small} VSG moment of inertia constant during deceleration (s^2)

K_Q VSG reactive power droop coefficient (pu)

K_V Droop parameter of voltage control (pu)

K_{dc} VSG adaptive damping controller gain

K_{I_I} Integral gain of VSC current control loop

K_{I_Q} AVR Integral gain

K_{I_V} Integral gain of VSC voltage control loop

$K_{I_{AVR}}$ Integral gain of the virtual AVR

$K_{I_{dc}}$ Integral gain of the PI controller of the dc-link regulator

$K_{I_{VFC}}$ Integral gain of voltage-frequency controller

K_I Integral gain of the local PI-controller of the frequency control loop of the distributed controller

K_{LP_l} Load scaling factors for active power demand

K_{P_I} Proportional gain of VSC current control loop

K_{P_Q} AVR Proportional gain

K_{P_V} Proportional gain of VSC voltage control loop

$K_{P_{AVR}}$ Proportional gain of the virtual AVR

$K_{P_{dc}}$ Proportional gain of the PI controller of the dc-link regulator

$K_{P_{gov}}$ Proportional gain of virtual governor

$K_{P_{VFC}}$ Proportional gain of voltage-frequency controller

K_P Proportional gain of the local PI-controller of the frequency control loop of the distributed controller

L_f Inverter output filter inductance (H)

L_{dc} DC DER output filter inductance (H)

P_o VSG reference power (pu)

$P_{MG_i^{'}}$ Maximum power capacity of the local MG (pu)

$P_{MG_j'}$ Maximum power capacity of neighbouring MG (pu)

Q_o VSG reference reactive power (pu)

R_f Inverter output filter resistance (Ω)

R_s Virtual Synchronous Resistance (pu)

R_{dc} DC DER output filter resistance (Ω)

V_o Reference terminal voltage of VSG (pu)

V_{dc_o} DC-link reference voltage (pu)

$V_{dc_{ref}}$ Reference rated voltage of the dc microgrid (pu)

V_{max} Maximum allowable dc voltage (pu)

V_{min} Minimum allowable dc voltage (pu)

X_s Virtual Synchronous Reactance (pu)

Variables

Δf System frequency deviation (Hz)

ΔP_D Change in the demand of voltage-dependent loads (pu)

ΔP_{MG_i} Local control signal tracking $\Delta P_{MG_{ref}}$ (pu)

ΔP_{MG_j} Output power variation of a neighbouring MG j (pu)

$\Delta P_{MG_{ref_i}}$ Reference power to be used in the inner power control loop of the distributed consensus controller (pu)

γ Actual measured frequency or dc voltage of the MG

$\gamma_i^{'}$ Normalized ac frequency or dc voltage index

ω_{PLL} Angular frequency obtained from the PLL (rad/s)

ω_{ref} Reference Angular velocity of the VSG (rad/s)

ω_{VSG} Angular velocity of the VSG (rad/s)

θ_R Virtual rotor angle (rad)

a_{LP} Filtered value of the derivative of the angular velocity of the VSG

E_d Virtual internal field voltage (pu)

I_c VSC output current before filter (pu)

I_d VSC output current d-component (pu)

I_g VSC output current after filter (pu)

I_L DC DER inductance current (pu)

I_q VSC output current q-component (pu)

I_{dco} d-component reference current for inner current control loop of VSG (pu)

I_{dc} VSG interface current from the dc side (pu)

I_{qco} q-component reference current for inner current control loop of VSG (pu)

$I_{d_{ref}}$ d-component reference current for inner current control loop of dc-link regulator (pu)

$I_{q_{ref}}$ q-component reference current for inner current control loop of dc-link regulator (pu)

P_e Output power of the VSG (pu)

P_{ac} VSG interface ac side power (pu)

P_{dc_L} DC load power (pu)

P_{dc} VSG interface dc side power (pu)

P_{gov} Input power obtained from the virtual governor (pu)

P_{ref} Reference active power of dc-link regulator (pu)

Q_{out} VSG reactive power output (pu)

Q_{ref} Reference reactive power of dc-link regulator (pu)

V Load voltage (pu)

V^* Reference voltage for VSG voltage regulator (pu)

V_d VSC output voltage d-component (pu)

V_d^* VSC d-component reference voltage for dq/abc conversion block (pu)

V_q VSC output voltage q-component (pu)

V_q^* VSC q-component reference voltage for dq/abc conversion block (pu)

V_{dc} DC link voltage (V)

V_{DER} DC DER voltage (pu)

V_{do} VSG d-component reference voltage for voltage control loop (pu)

V_{out} VSG output voltage (pu)

V_{qo} VSG q-component reference voltage for voltage control loop (pu)

1. Introduction

Microgrids (MGs) are a promising solution to tackle the reliability, economic, and environmental issues associated with conventional power networks that mainly rely on centralized power stations to fulfill consumers' power demands [1]. These systems consist of clusters of loads and Distributed Energy Resources (DERs) interconnected through medium and low voltage distribution feeders, capable of working in grid-connected mode and isolated mode, which when interconnected form Active Distribution Networks (ADNs) that enhance power system operation and reliability.

The proliferation of ac and dc MGs may result in the formation of a distribution network with feeders and interconnected MGs or a grid of MGs, referred here as Multi-MG (MMG) systems, which are capable of large-scale integration of DERs that require frequency and voltage control coordination. In this context, the power mismatches within the ac/dc MGs could be mitigated by exchanging power with the rest of the system through an ac host grid, providing/receiving ancillary services to/from other ac and dc MGs and/or the host grid, while ensuring optimal power-sharing among the MGs to maintain the power balance of the overall system [2]. Hence, a combination of control techniques and network architectures could be utilized to improve the system's power-sharing capability and the overall system frequency and voltage control, thus enhancing the integrated system's stability and reliability.

The majority of MG studies in the literature mainly address the control and coordination of single isolated MGs, which are being standardized [3], with a few studies focused on addressing technical issues in MMG systems. The latter focus mainly on the development of Energy Management Systems (EMS) and optimization techniques for steady-state control, assuming that the MGs are interconnected together through a host network (e.g, [4, 5]), with some papers addressing dynamics and control of MMGs, such as [6, 7, 8], which propose active power coordination techniques for interconnected MGs. The network topologies in these studies assume that ac MGs are directly interconnected without a power electronic-based interface, which significantly limits the controllability of the power exchanged among the MGs, especially in the case of a weak host grid; thus, if a disturbance occurs in an MG, the whole system is affected, since the frequencies and voltages of the MGs are not decoupled. These studies also assume a simplified model for the MGs, which ignores the non-linearity of these systems by neglecting the voltage dependency of the loads, and model the MGs either as a first-order transfer function or as a single DER, which do not properly represent the actual and complex dynamics of isolated MGs.

Relevant studies that involve dynamic modeling and control of networks of multiple dc MGs are presented in [9, 10, 11]. In these studies, the authors propose coordination techniques to adjust DER dc voltage setpoints for each MG in the network; however, they do not consider the possibility of having ac MGs in the integrated system. Furthermore, several simplifications are made, such as representing MGs as a single DER with a dc-dc converter and a load, without considering the dynamics of converter-interfaced loads, which have a detrimental impact on the stability of the system by inducing voltage oscillations, especially if dc line inductances are considered, which may resonate with DER filters [12, 13].

Studies that consider interconnecting MMGs through power-electronics-based interfaces are presented in [14, 15]. Thus, the authors in [14] discuss an interface that connects each ac MG in the system with the host grid through switches, and interconnects the cluster of MGs directly through a dc link with a Battery Energy Storage System (BESS). This hybrid ac/dc connection offers several benefits, such as mitigation of synchronization problems, and better control and power-sharing among the interconnected MGs. However, dc MGs, which present different dynamics, are not considered as part of the overall system. The study in [15] proposes a similar interconnection for power sharing among ac and dc MGs. The coordination techniques proposed in these studies are only suitable for the specific network topologies presented, which hinders the coordination techniques' scalability; furthermore, the proposed interconnection approaches in these papers would be costly for large MMG systems, due to the need to add dc lines with BESSs.

To address the aforementioned limitations in the existing literature associated with control and dynamics of MMG systems that contain both ac and dc MGs, this paper proposes the use of ac-dc-ac and dc-ac converter interfaces for the interconnection of the ac and dc MGs, respectively, to properly control the interfaces and the individual MGs. It also proposes a new hierarchical distributed control approach for the proper exchange of power among the MGs, considering and improving the overall system frequency

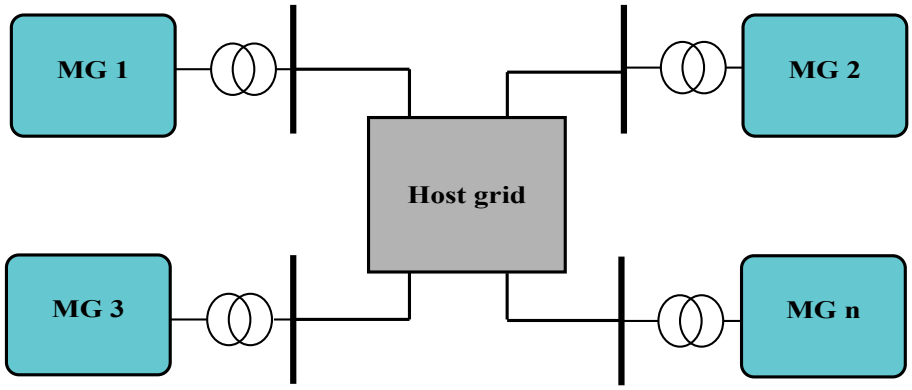


Figure 1: Typical topology of a grid of microgrids [2].

and voltage control. Virtual Synchronous Generator (VSG) techniques are used in the proposed interface converters to adaptively adjusts the inertia and damping constants, while considering Voltage Frequency Control (VFC) to improve the frequency and voltage stability of the system. Thus, the following are the main contributions of this paper:

- A new adaptive inertia and damping control with VFC for VSG-based interfaces of ac MGs, which enhances the frequency response of the ac MGs and the ac host grid in a MMG system, limiting frequency excursions, especially during severe disturbances, and allowing proper power sharing among the MGs without causing significant power transients.
- A novel control for VSG-based dc-ac interfaces of dc MGs with adaptive damping to improve the dc MG voltage dynamics.
- A new distributed controller for the MMG system, which coordinates the power exchanged through the ac and dc MG interfaces to maintain the power balance of the overall system. The developed controller coordinates the system based on limited information, which improves its scalability to larger MMG systems and improves its robustness to single point failures.

The rest of the paper is organized as follows: Section 2 briefly discusses basic concepts of MMGs and VSGs. Section 3 introduces and explains the proposed VSG-based interfaces for both ac and dc interfaces, based on adaptive inertia and damping as well as VFC, and a decentralized control approach for the distributed ac and dc MG interface controllers. Section 4 presents and discusses several time-domain simulations for various case studies on an MMG test system, based on a CIGRE benchmark ADN, demonstrating, validating, and comparing the proposed methods with respect to a standard droop control approach. Finally, Section 5 highlights the main conclusions and contributions of the presented work.

2. Background Review

2.1. Multi-Microgrid (MMG) Systems

MMG systems are a relatively new field of research in power systems, which has gained momentum in recent years due to the rapid proliferation of MGs. It is based on a grid with multiple interconnected MGs to facilitate the integration, control, and coordination of intermittent DERs within a power system, by adequately managing these resources within each MG for a more efficient overall utilization of DERs [2]. A typical layout of an MMG system consists of several MGs, each connected at their point of common coupling to a host grid, which links them all, as shown in Figure 1. In this paper, the ac host grid is assumed to have limited small inertia, to represent, for example, an ADN with multiple ac and dc MGs and a weak or

non-existent connection to the transmission system, since such a system would be inherently less stable and thus present a more challenging control problem.

2.2. Virtual Synchronous Generators (VSGs)

The proposed converters that interface the considered ac and dc MGs in this paper are assumed to have a control system that behaves like a Synchronous Generator (SG), by emulating its inertia and damping characteristics through the implementation of the SG swing equation in the controllers of the interfacing Voltage Source Converters (VSCs) [16]. Several models have been proposed in the literature to reproduce the dynamics of SGs in VSCs, most of which are voltage controlled, making them susceptible to faults due to the lack of current control loops. Other techniques are based on current control VSCs, which are dependent on a Phase Locked Loop (PLL) for synchronization with the grid. The control architecture used here is based on [17, 18], which overcomes the aforementioned issue and consists of robust cascaded control loops, where a voltage control loop utilizes the virtual rotor angle as a reference that is generated by the internal swing equation model, cascaded with a current control loop. However, in these papers, the proposed VSG is not considered in the context of Back-to-Back (B2B) converter interfaces, and the operational constraints of the VSC dc side and the VSG AVR are not considered, which are all issues addressed for the first time in the current paper to improve the overall dynamic response of MMG systems.

2.3. VSG Governor and AVR Model

The generic architecture of a VSG is derived from [18], consisting of several control loops such as an AVR, the VSG swing equation that includes the governor, a virtual synchronous impedance, and standard VSC voltage control and current control loops [19], as explained next. Thus, the VSG is centered on the virtual implementation of the following and physical SG swing equation with no approximations [16]:

$$P_{gov} - P_e = J_{ac}\omega_{VSG}\frac{\mathrm{d}\omega_{VSG}}{\mathrm{d}t} + D_{ac}(\omega_{VSG} - \omega_{PLL}) \tag{1}$$

$$\frac{\mathrm{d}\theta_R}{\mathrm{d}t} = \omega_{VSG} \tag{2}$$

where P_{gov} is the input power obtained from the virtual governor, P_e is the output power of the VSG, J_{ac} is the virtual moment of inertia, D_{ac} is the virtual damping factor, ω_{VSG} is the angular velocity of the VSG, ω_{PLL} is the angular frequency obtained from the PLL, and θ_R is the virtual rotor angle, which is fed to the dq/abc and abc/dq conversion blocks to synchronize the VSG to the grid.

The VSG governor includes a droop control to implement the frequency-power relationship in SGs to share the load demand proportionally among the VSGs, which yields the following virtual prime-mover power P_{gov} in the swing equation:

$$P_{gov} = \frac{K_{P_{gov}}(\omega_{ref} - \omega_{VSG})}{1 + \tau_{gov}s} + P_o \tag{3}$$

where $K_{P_{gov}}$ is the VSG droop coefficient, P_o is the VSG reference power, and τ_{gov} is a virtual turbine and governor time constant.

The AVR generates the VSG field voltage E_d, and is used to implement the voltage-reactive power relationship through a droop control as follows:

$$E_d = \left[K_Q(Q_o - Q_{out}) + V_o - V_{out}\right]\left(K_{P_Q} + \frac{K_{I_Q}}{s}\right) \tag{4}$$

where Q_o is the reference reactive power, Q_{out} is the reactive power output, K_Q is the droop coefficient, V_o is the reference terminal voltage, V_{out} is the VSG output voltage, and K_{P_Q}, and K_{I_Q} are the gains of the AVR PI controller.

2.4. Virtual Synchronous Impedance and Voltage Control Loops

The virtual internal field voltage E_d generated by the AVR is behind a virtual synchronous impedance $R_s + jX_s$, which is fed to the voltage control loop to regulate the terminal voltage of the VSG. Thus, the following are the reference input voltages V_{do} and V_{qo} for the voltage control loop:

$$V_{do} = E_d + X_s I_q - R_s I_d \quad (5)$$

$$V_{qo} = 0 - X_s I_d - R_s I_q \quad (6)$$

These are then utilized in the voltage control loop to generate the dq-axis components of the reference currents for the inner current control loop as follows:

$$I_{dco} = (V_{do} - V_d)\left(K_{P_V} + \frac{K_{I_V}}{s}\right) - V_q\ \omega_{VSG}\ C_f + I_d\ G_{ff}(S) \quad (7)$$

$$I_{qco} = (V_{qo} - V_q)\left(K_{P_V} + \frac{K_{I_V}}{s}\right) + V_d\ \omega_{VSG}\ C_f + I_q\ G_{ff}(S) \quad (8)$$

where $G_{ff}(S)$ is a first-order transfer function of a feed-forward filter, I_d and I_q are the dq components of the output current, and K_{P_V} and K_{I_V} are the parameters of the PI controller of the voltage control loop. The reference currents have hard-limits to protect the VSC from overcurrents.

2.5. Current Control Loop

The inner current control loop generates the decoupled dq components V_d^* and V_q^*, which are fed to the dq/abc conversion block to be used as a reference for the VSC, as follows:

$$V_d^* = (I_{dco} - I_{dc})\left(K_{P_I} + \frac{K_{I_I}}{s}\right) - I_{qc}\ \omega_{VSG} L_f + V_d\ G_{ff}(S) \quad (9)$$

$$V_q^* = (I_{qco} - I_{qc})\left(K_{P_I} + \frac{K_{I_I}}{s}\right) + I_{dc}\ \omega_{VSG} L_f + V_q\ G_{ff}(S) \quad (10)$$

where K_{P_I} and K_{I_I} the parameters of the PI controller of the current control loop. It should be mentioned that for the type of control and stability issues studied here, given the time constants of the phenomena considered, an average model of the VSC suffices, without the need to consider the converter switching controls, as discussed in [20].

3. Proposed Microgrid Interfaces and Controls

The proposed control scheme interfaces the dc and ac MGs with the ac host grid through a VSG controller. This approach offers several advantages, such as full controllability of the power flow among the linked MGs, while decoupling the frequencies of ac MGs and the voltage of dc MGs, thus allowing MGs to operate at different frequencies or dc voltages, and minimizing the impact of disturbances on the MGs. This also allows providing virtual inertia and damping by implementing the aforementioned VSG control approach in the B2B converters, which may be modulated as proposed here to improve the frequency response of the overall system.

3.1. B2B VSG Interface

The proposed B2B interface used for all ac MGs in the MMG system consists of two VSCs connected through a DC-Link as depicted in Figure 2 [19], where each VSC includes the control loops discussed in Section 2, plus the controls proposed and described next. Thus, the left-hand side connects to the MG, while the right-hand side connects to the ac host grid, with both VSCs being capable of operating in VSG mode and regulating the DC-Link voltage, depending on the following proposed coordination technique for the MMG system: If the ac MG needs frequency regulation, the left-hand side VSC operates in VSG mode and provides frequency support for the MG, while the right-hand side regulates the DC-Link voltage. If the MG has excess generation capacity from its DERs, it can export power to the rest of the system by operating the right-hand-side in VSG mode, while the left-hand-side VSC regulates V_{dc}.

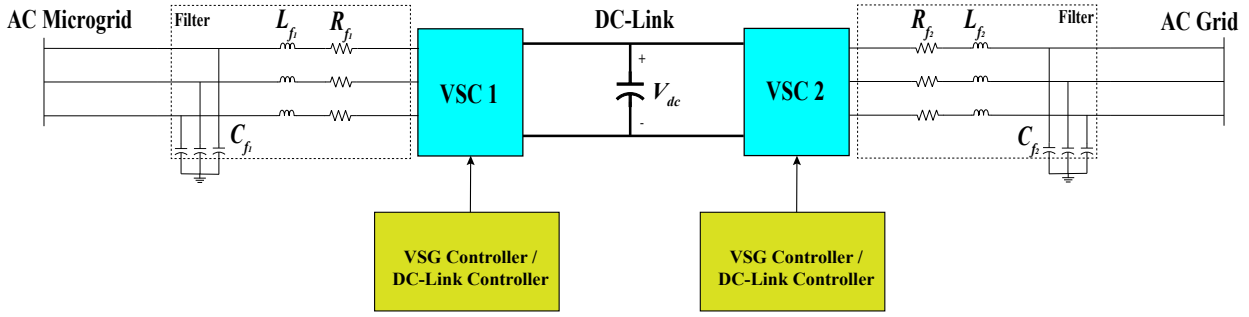


Figure 2: Proposed B2B VSG interfaces, with each VSC operating as a VSG or a dc link regulator [19].

3.1.1. DC-Link Voltage Regulation

The VSC that regulates V_{dc} works in current control mode, controlling the active power output of the VSC to satisfy the power balance of the DC-Link and maintain a constant dc voltage. The dq-components of the reference currents in this case may be calculated as follows [19]:

$$I_{d_{ref}} = \frac{2}{3}\frac{P_{ref}V_d + Q_{ref}V_q}{V_d^2 + V_q^2} \tag{11}$$

$$I_{q_{ref}} = \frac{2}{3}\frac{P_{ref}V_q - Q_{ref}V_d}{V_d^2 + V_q^2} \tag{12}$$

where V_d and V_q are the dq-components of the output voltage, and P_{ref} and Q_{ref} are the desired active and reactive power, respectively, with P_{ref} being obtained from the DC-Link voltage regulator loop as follows:

$$P_{ref} = -\left(V_{dc_o}^2 - V_{dc}^2\right)\left(K_{P_{dc}} + \frac{K_{I_{dc}}}{s}\right) + P_{dc} \tag{13}$$

where V_{dc_o} is the reference DC-Link voltage, V_{dc} is the actual DC-Link voltage, $K_{P_{dc}}$ and $K_{I_{dc}}$ are the parameters of the PI controller of the dc link regulator loop, and P_{dc} is the feed-forward term that represents the DC-Link power, which is approximately equal to the output power of the other VSC that is operating in VSG mode.

The reference currents $I_{d_{ref}}$ and $I_{q_{ref}}$ are inputs for the current control loop with decoupling feed-forward terms to obtain the dq-axes voltage references, which are fed to the VSC in Figure 3 after transformation to the abc-reference frame, as follows [21]:

$$V_d^* = \left(I_{d_{ref}} - I_d\right)\left(K_{P_I} + \frac{K_{I_I}}{s}\right) - I_q\omega L_f - V_q\ \omega C_f R_f + V_d(1 - \omega^2 L_f C_f) + I_d R_f \tag{14}$$

$$V_q^* = \left(I_{q_{ref}} - I_q\right)\left(K_{P_V} + \frac{K_{I_I}}{s}\right) + I_d\omega L_f + V_d\ \omega C_f I_d + V_q(1 - \omega^2 L_f C_f) + I_q R_f \tag{15}$$

The parameters of the PI controllers of the DC-Link voltage regulator and the current control loop are tuned to ensure the control loops are stable when the VSC injects or absorbs its rated power [22].

3.1.2. VFC

It is usually assumed that reactive power does not impact the DC-Link power balance, since it is produced from the exchanged energy among the phases of the VSC [19]. However, in ac MGs, loads are typically voltage-dependent, and hence, with suitable voltage control, the frequency of the MG could be controlled by controlling the operating voltage of the MG, minimizing the impact of disturbances on the system and creating more active power reserves, thus allowing the VSG interface to export more power to the rest of the system. Therefore, the previously discussed AVR of the VSG is augmented here with a VFC controller

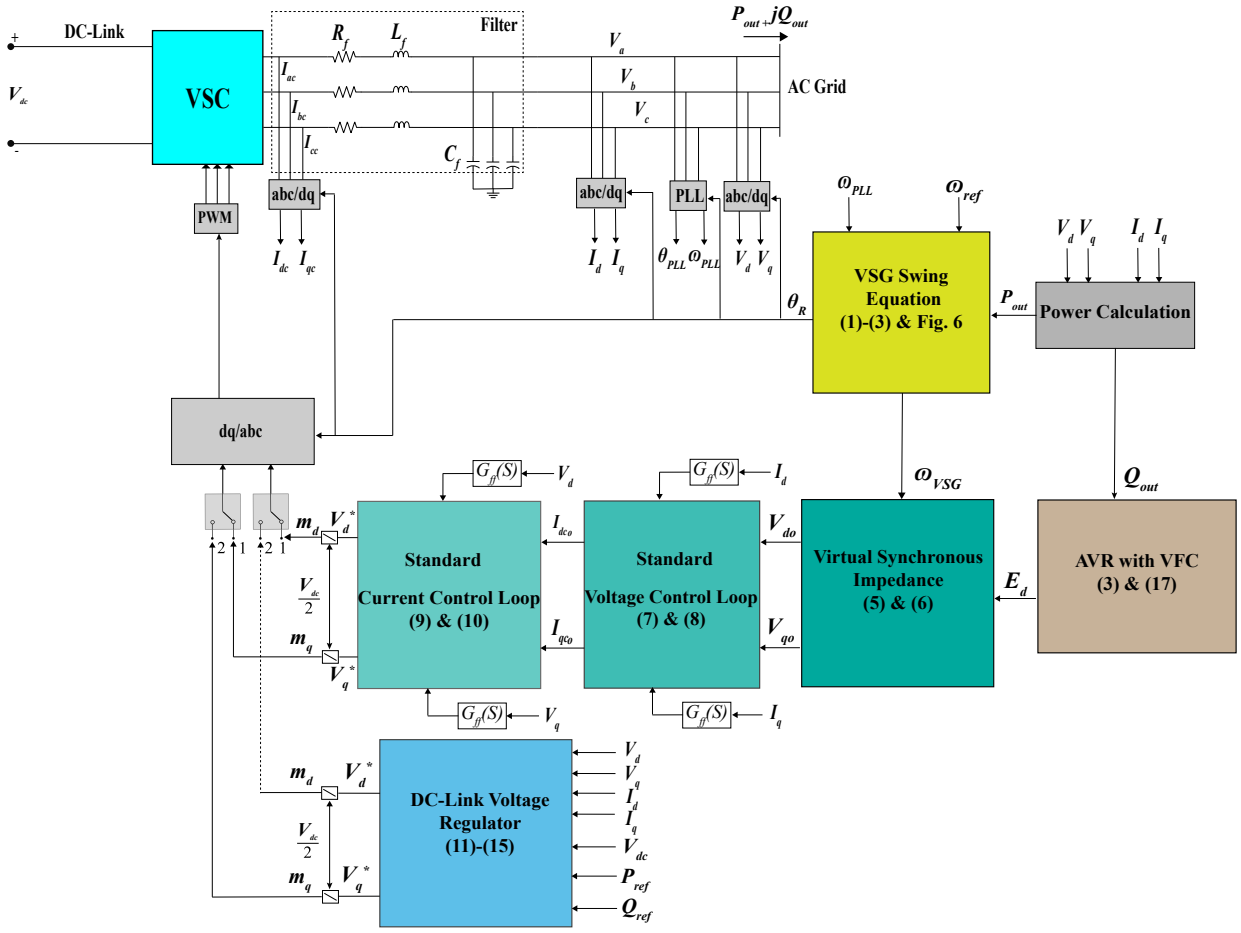


Figure 3: VSCs of ac MG B2B interfaces with proposed VSG and DC-Link controls. Depending on the power flow through the interface, the switches position 1 activates the VSG controls, whereas position 2 activates the DC-Link control.

based on [23], considering that the load powers of the MG are represented by an exponential model. Thus, adjusting the voltage setpoints of the DERs and the B2B VSC affects the total MG load demand ΔP_D as follows:

$$\Delta P_D = \sum_{l=1}^{N_L} K_{P_l} \left[(V + \Delta V)^{\alpha_{P_l}} - V^{\alpha_{P_l}} \right] \tag{16}$$

where K_{P_l} and α_{P_l} are the parameters of the l^{th} exponential load power $K_{P_l} V^{\alpha_l}$, and V is the ac MG voltage, neglecting its grid as in [23]. The frequency of the system could then be controlled by adjusting the change in the operating voltage of the MG as follows:

$$\Delta V = \left(K_{P_{VFC}} + \frac{K_{I_{VFC}}}{s} \right) \frac{1 + \tau_{1_Q} s}{1 + \tau_{2_Q} s} \Delta f \tag{17}$$

where $K_{P_{VFC}}$ and $K_{I_{VFC}}$ are the parameters of a PI controller, and τ_{1_Q} and τ_{2_Q} are lead-lag time constants. It is important to note that the VFC does not only provide frequency regulation by adjusting the voltage setpoints, but also enhances the VSG fault ride-through by reducing output voltage during faults. The proposed VFC is integrated into the AVR of the VSG interface as shown in Figure 4, where the reactive power droop controller is cascaded by a VFC, which generates the reference voltage V^* for the voltage

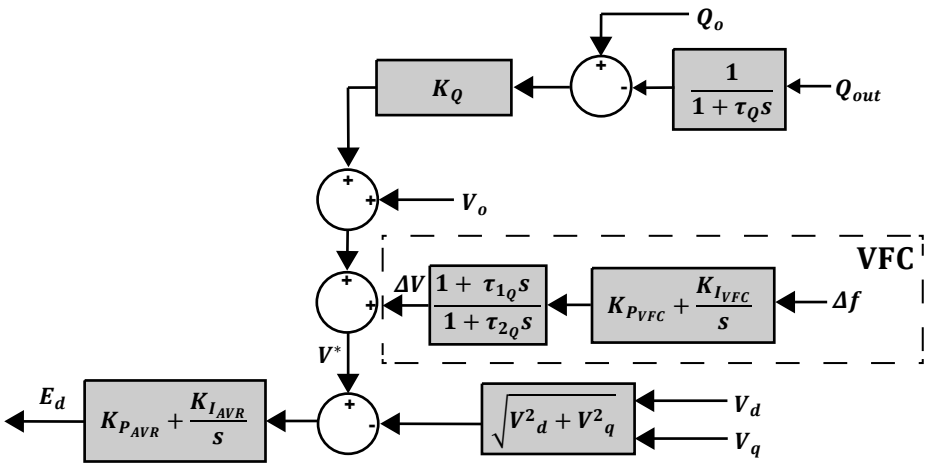


Figure 4: AVR of the VSG interface with VFC to regulate MG frequency through voltage control.

Frequency	$\mathrm{d}\omega_{VSG}/\mathrm{d}t$	Mode	Inertia	Damping
$f \geq f_{min}$	$\lvert a_{LP}\rvert \uparrow$	Accel.	$J_{big}+a_{LP}$	D_o
$f \geq f_{min}$	$\lvert a_{LP}\rvert \downarrow$	Decel.	J_{small}	D_o
$f \leq f_{min}$	$\lvert a_{LP}\rvert \uparrow$	Fault	J_{small}	$D_{big}+a_{LP}$

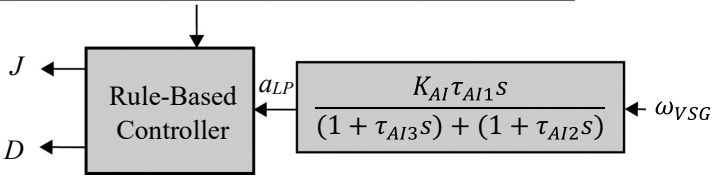


Figure 5: Proposed rule-based VSG adaptive inertia to curb frequency excursions.

regulator as follows:

$$V^* = V_o + \Delta V + K_Q\left(Q_o - \frac{Q_{out}}{1+\tau_Q s}\right) \tag{18}$$

Here, τ_Q represents the reactive power measuring delays. The regulator then utilizes a PI controller with corresponding gains $K_{P_{AVR}}$ and $K_{I_{AVR}}$ to generate the virtual internal field voltage E_d as follows:

$$E_d = \left(K_{P_{AVR}} + \frac{K_{I_{AVR}}}{s}\right)(V^* - V) \tag{19}$$

3.1.3. Adaptive Inertia

Unlike conventional SGs, the inertia and damping characteristics of the VSG could be adjusted with a suitable controller to obtain an optimal frequency response and enhanced stability. The technique proposed here is based on adjusting the inertia constant of the VSG as discussed in [24]; however, that approach has some limitations, since it alternates the inertia constant between a large inertia J_{big} during acceleration of the VSG and a small inertia J_{small} during deceleration of the VSG, independent of the operating condition of the system and the severity of the disturbance. Furthermore, the damping constant of the virtual swing equation is not utilized to further improve the dynamic response of the system.

The control technique proposed here adjusts the values of the inertia and the damping constants using the rule-based approach shown in Figure 5, based on a low pass filtering of the measured rate of change of the ω_{VSG}, with parameters K_{AI} and τ_{AI}s, which is more accurate and requires less measurement than the method presented in [24]. Thus, the proposed controller samples and filters the absolute value of the

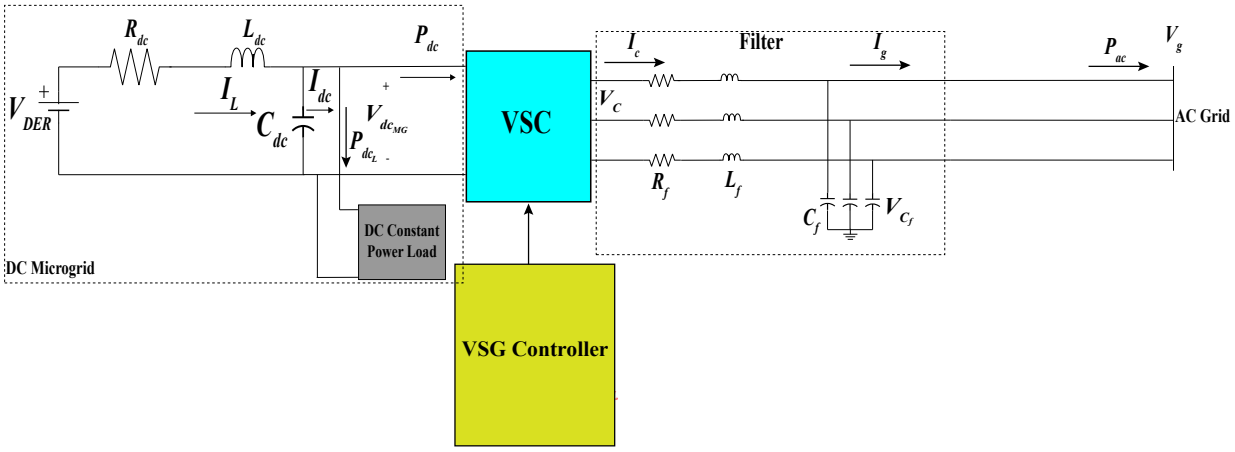


Figure 6: Proposed dc MG VSG interface with adaptive damping to limit dc MG voltage oscillations.

derivative of the angular velocity of the VSG, yielding a_{LP} in Figure 5 to determine if the VSG is accelerating or decelerating and to capture the severity of the disturbance. If the VSG is accelerating, a large inertia constant J_{big} (e.g., $J_{big} = 10J_o$) is chosen, while also adding a_{LP} to reflect the disturbance stress; this slows the VSG and limits further frequency excursions. Otherwise, a small inertia constant J_{small} (e.g., $J_{small} = J_o/50$) is chosen to speed up the recovery of the frequency of the system. However, if the frequency at the converter regulating the dc voltage drops below a minimum frequency (e.g., $f_{min} = 59.8$ Hz), the controller chooses a large value for the damping constant D_{big} (e.g., $D_{big} = 3D_o$), and adds a_{LP} to reflect the disturbance severity, while reducing the inertia constant to its minimum value J_{small}, as illustrated in Figure 5, which makes the VSI on the VSG side sluggish, thus reducing its power draw. This will have a stabilizing effect on the system regulating the dc voltage, especially during disturbances, since it would mitigate the possible collapse of the DC-Link voltage of the B2B converter, and prevent frequency or voltage collapse on a system that does not have enough generation capacity to regulate the DC-Link.

3.2. DC MG Interface

The interface that connects the dc MGs to the MMG system is shown in Figure 6. The VSC converter in this case utilizes a different VSG control with VFC than the B2B, as explained next.

The presence of converter interfaced loads in dc MGs have a detrimental impact on the stability of the system, since they effectively act as constant power loads, resulting in a negative incremental impedance that causes significant voltage and power oscillations in these MGs [12, 13]. Thus, the dc converter interface can contribute to reducing voltage oscillations in dc MGs if a proper controller is utilized. In this case, the impact of a VSG dc MG interface on the dynamics of the dc MG can be considered based on the following equations that represent the dynamics of the dc currents and voltages of the average converter model:

$$L_{dc}\frac{\mathrm{d}I_L}{\mathrm{d}t} = V_{DER} - R_{dc}I_L - V_{dc_{MG}} \tag{20}$$

$$C_{dc}\frac{\mathrm{d}V_{dc_{MG}}}{\mathrm{d}t} = I_L - I_{dc} \tag{21}$$

$$I_{dc} = \frac{P_{dc_L} + P_{dc}}{V_{dc_{MG}}} \tag{22}$$

$$J_{dc}\omega_{VSG}\frac{\mathrm{d}\omega_{VSG}}{\mathrm{d}t} = P_{gov} - P_{dc} - D_{dc}\Delta\omega_{VSG} \tag{23}$$

$$C_f\frac{\mathrm{d}V_{C_f}}{\mathrm{d}t} = I_c - I_g \tag{24}$$

$$L_f\frac{\mathrm{d}I_c}{\mathrm{d}t} = V_c - R_f I_c - V_{C_f} \tag{25}$$

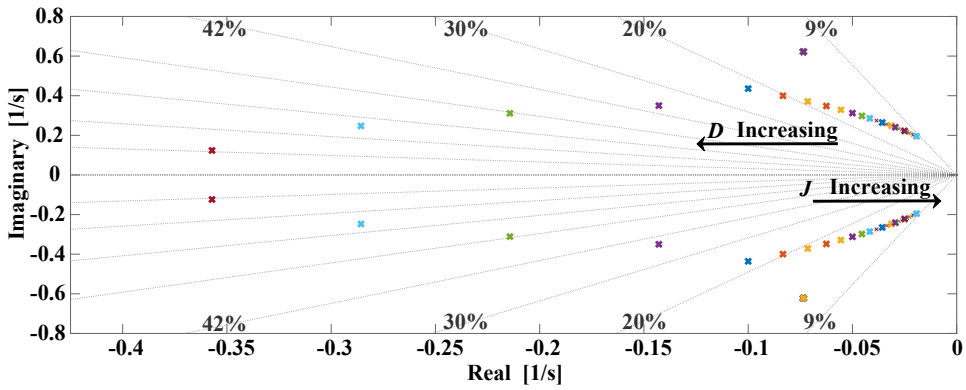


Figure 7: Example of impact of damping and inertia constant on dominant eigenvalues for the VSG dc MG interface.

where $V_{dc_{MG}}$ is the dc MG voltage, and P_{dc} is the converter's dc side power, which for an average model of the converter is equal to P_{ac} when neglecting converter losses; the rest of the parameters and variables not previously defined are found in Figure 6. A set of state-space linear time-invariant first order differential equations can be obtained from equations (20)-(25) as follows:

$$\Delta\dot{x} = \mathcal{A}\Delta x + \mathcal{B}\Delta u \tag{26}$$

$$\Delta y = \mathcal{C}\Delta x + \mathcal{D}\Delta u \tag{27}$$

Based on this linear model, the impact of damping and inertia constant on the dominant eigenvalues can be obtained. Thus, it can be observed from sample simulations, as shown in Figure 7, that increasing the damping shifts the dominant eigenvalues to the left in the complex plane, leading to a more stable system, while increasing the inertia constant shifts the dominant eigenvalues to the right, resulting in oscillatory modes. Hence, for a given fixed J_{dc} (unlike the adaptive J_{ac} in the B2B interface), the proposed controller for the dc-ac converter should adaptively adjust the damping constant as a function of the absolute value of the rate of change of the VSG angular velocity, so that the VSG damping of the dc MG interface increases, as follows:

$$D_{dc} = \frac{1+\tau_{dc_1}s}{1+\tau_{dc_2}s}\frac{K_{dc}s}{1+\tau_{dc}s}|\Delta\omega_{VSG}| + D_o \tag{28}$$

where D_o is a nominal value of the damping constant, and K_{dc} and the τ_{dc}s are gains and time constants that need to be properly tuned. This controller ensures that the interface power exchanges with the rest of the system do not result in significant dc-voltage transients. This interface also includes the previously discussed virtual impedance and AVR controls, and may also include VFC to improve the frequency regulation of the ac host grid.

3.3. Distributed Control System

A distributed droop-free frequency and dc-voltage control that fulfills the role of secondary control is developed in this section to coordinate the MMG system by controlling the output powers of the MG VSG interfaces. The technique is derived from the distributed consensus technique proposed in [25], which is modified to coordinate both ac and dc MGs in the MMG system.

3.3.1. Communication Graph

Based on bidirectional communication, the proposed distributed control consists of a control layer which is associated with a communication graph. The aim of the controller is to coordinate the output powers of the ac and dc MGs, and thus the interfacing VSGs are linked with communication channels to exchange coordination information. Two sets of vectors are used to represent a graph $G = (\mathcal{V}, \mathcal{E})$, where $\mathcal{E}$ represents the links from node v_i to node v_j, while the set $\mathcal{V}$ contains the vertices or nodes of the graph $[v_1, v_2, .., v_N]$,

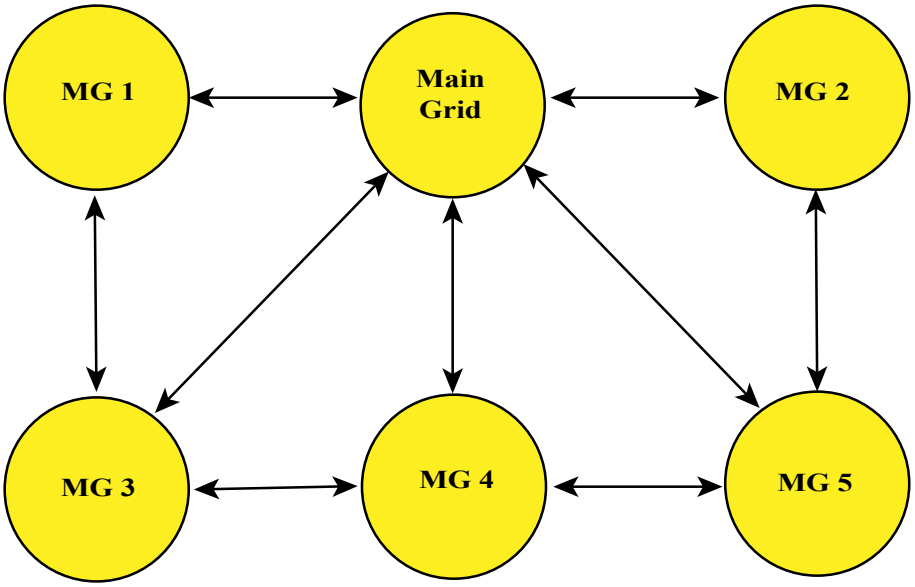


Figure 8: Example of the communication topology for the proposed distributed controller.

corresponding only to the interfacing VSGs of the interconnected MGs. A connectivity matrix $A_G = [a_{ij}]$ can be defined, with weights $a_{ij} = 0$ if MG i does not exchange information with MG j, or $a_{ij} = 1$ if a link $(v_i, v_j) \in \mathcal{E}$ exists.

The proposed communication topology to coordinate the MMGs includes spanning trees to minimize the impact of communication link failures, and reflects the MGs geographical placements. In this topology, the communication links among the MGs are bidirectional, and each MGs can communicate only with neighboring MGs, while the host grid communicates bidirectionally with all MGs. Thus, the connectivity matrix for the example illustrated in Figure 8 can be defined as follows:

$$A_G = \begin{array}{c} \begin{matrix} MG1 & MG2 & MG3 & Main & MG4 & MG5 \end{matrix} \\ \begin{bmatrix} 0 & 0 & 1 & 1 & 0 & 0 \\ 0 & 0 & 0 & 1 & 0 & 1 \\ 1 & 0 & 0 & 1 & 1 & 0 \\ 1 & 1 & 1 & 0 & 1 & 1 \\ 0 & 0 & 1 & 1 & 0 & 1 \\ 0 & 1 & 0 & 1 & 1 & 0 \end{bmatrix} \end{array} \begin{matrix} MG1 \\ MG2 \\ MG3 \\ Main \\ MG4 \\ MG5 \end{matrix} \tag{29}$$

Based on this communication graph approach, the controller coordinates the output powers of the MGs, with interfacing VSGs being linked with communication channels to exchange coordination information.

3.3.2. Adaptive Distributed Control

The proposed distributed consensus controller relies on a rule based technique to coordinate the output powers of the MGs, which is based on the following normalized index γ_i' of frequencies for ac MGs and dc voltages for dc MGs:

$$\gamma_i' = \frac{\gamma_i - \gamma_{min}}{\gamma_{max} - \gamma_{min}} \tag{30}$$

where γ_i is the actual frequency or dc voltage of MG i, and γ_{max} and γ_{min} are the maximum and minimum allowable frequency or dc voltage deviations. Thus, if $\gamma_i' > 0$, MG i has excess power, with the MG acting as a source through its VSG interface, which is controlled by the distributed consensus controller described

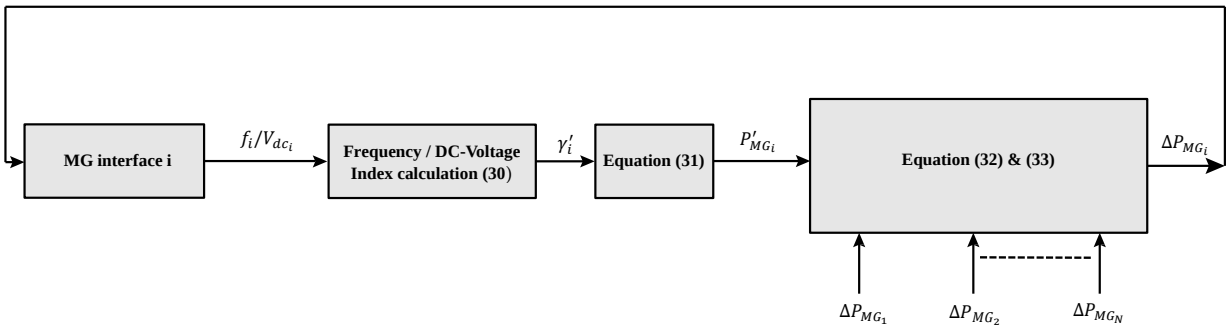


Figure 9: Proposed MMG distributed controller to regulate MG frequencies and voltages.

next. If $\gamma'_i < 0$, MG i has a power deficiency due to not enough generation to supply local demand, with the MG being considered a controllable load in this case. If $\gamma'_i = 0$, then there is no power exchange with the MMG, as either the ac frequency of the MG is at f_{min} (e.g., 59.8 Hz as per [3]), or the dc voltage of the MG is at its minimum steady state value V_{min} (e.g., -10% voltage deviation as per [26]). If $\gamma'_i = 1$, either the ac frequency of the MG is at its maximum value (e.g., 60.2 Hz as per [3]) or the dc voltage of the MG is at its maximum value (e.g., +10% as per [26]).

3.3.3. Rule Based Controller

Unlike the distributed control technique proposed in [25], which only coordinate the DERs of a single MG, the proposed controller here coordinates the MMG system to regulate both the frequencies of ac MGs and the voltages of dc MGs. Thus, the proposed distributed consensus control is activated for an MG when its $\gamma'_i > 0$, in which case:

$$P'_{MG_i} = \gamma'_i \overline{P_{MG_i}} \tag{31}$$

where $\overline{P_{MG_i}}$ is the maximum output power of the interfacing VSG, and P'_{MG_i} is used in the distributed consensus controller to share the power proportionally among the MGs. In this case, the MGs coordinate their output power though the following local frequency control loop:

$$\Delta P_{MG_{ref_i}} = (\gamma'_o - \gamma') \left(K_P + \frac{K_I}{s} \right) \ \forall i \tag{32}$$

$$\Delta P_{MG_i} = \frac{1}{s} \left[\sum_{j \in N_i} a_{ij} \left(\frac{\Delta P_{MG_j}}{P'_{MG_j}} - \frac{\Delta P_{MG_i}}{P'_{MG_i}} \right) + b_i \left(\Delta P_{MG_{ref_i}} - \frac{\Delta P_{MG_i}}{P'_{MG_i}} \right) \right] \ \forall i \tag{33}$$

where γ'_o is the index value corresponding to the nominal frequency $\gamma_o = f_o$ of the ac host grid; γ' is the measured frequency index of the host grid; K_P and K_I are the parameters of the local PI-controller of the frequency control loop; and $\Delta P_{MG_{ref_i}}$ is the reference power used in the inner power control loop equation (33) of the distributed consensus controller.

In (33), the output powers of neighbouring interfacing VSGs are communicated to the local VSG interface i, to be used in the inner power control loop. In this equation, ΔP_{MG_i} represents the local control signal tracking $\Delta P_{MG_{ref_i}}$ for MG i; ΔP_{MG_j} is the output power variation of a neighbouring MG j; P'_{MG_i} and P'_{MG_j} are the maximum power capacities of the local MG and neighbouring MG, respectively, which are modulated by the frequency or dc-voltage index of the corresponding MG as per (31); a_{ij} is either 1 or 0, depending on the communication network linking the interfacing VSGs, as explained in the previous section; and b_i is set to 1 to account for the local $\Delta P_{MG_{ref_i}}$ signal in the VSG inner control loop. This equation results in the convergence of ΔP_{MG_i} to $\Delta P_{MG_{ref_i}}$. The proposed distributed controller is implemented as shown in Figure 9.

If the MGs have an index $\gamma'_i < 0$, the MG acts as a controllable load. In this case, the interfacing VSG regulates the frequency or the dc voltages as a function of the frequency index of the host grid, such that if

its frequency decreases, the power exchange from the main grid to the MG that acts as a load decreases as follows:

$$\Delta P_{MG_{ref_i}} = (\gamma' - \gamma'_i)\left(K_P + \frac{K_I}{s}\right) \ \forall i \tag{34}$$

The proposed controllers are integrated into the VSG shown in Figure 3 to control the VSG reference power P_o in (3), inside the VSG governor block. Note that the DERs within the MGs utilize droop control and VFC to regulate the frequency of ac MGs and the dc voltages in dc MGs.

4. Case Studies and Results

The proposed VSG-based interface and the aforementioned controllers are tested, validated, and compared on an MMG system derived from a CIGRE benchmark MG test system, which has been used for several MG studies [20, 21, 23, 27]. The topology of the MMG is depicted in Figure 10, which has been implemented for time-domain simulations in PSCAD [28], which is the best approach to study control performance and stability in MGs [20]. It consists of five MGs, two of which are dc MGs while the rest are ac MGs. DC MG 1 consist of a 1151 kW converter-interfaced load with power controls, two BESSs rated at 431 kW each, and a solar PV DER rated at 520 kW; dc MG 2 consist of a 1391 kW converter-interfaced load with power controls, two BESSs rated at 481 kW each, and a solar PV DER rated at 600 kW; ac MG 1 consist of a 1266 kW voltage dependent load, a 1040 kVA Diesel Generator (DG), a 212 kW BESS, and a 485 kW Wind Generator (WG); ac MG 2 consist of a 1091 kW voltage dependent load, a 978 kVA DG, a 212 kW BESS, and a 485 kW WG; and ac MG 3 consist of a 1260 kW voltage dependent load, a 1040 kVA DG, a 212 kW BESS, and a 485 kW WG.

The WGs in all MGs are assumed to be Type 4, modeled as explained in [21], and are operated at unity power factor. The ac loads are assumed to be unbalanced as in the original CIGRE MG system, modeled as explained in [23], and consist of 60% constant impedance load, 30% constant current load, and 10% constant power load. The dynamic models of the DERs in ac MGs are the same as the ones used in the original CIGRE MG system [21, 23], while the dc MG DERs are based on averaged models [29]. The rating of the VSG-based MG interfaces is 1.5 MW, and modeled as discussed in Section 3. All data for the test system and the controllers can be found in [30].

The proposed VSG-based interface's performance along with the proposed controllers, are compared through the following case studies:

- Case 1: Corresponds to the MG interfaces integrated into the host grid using frequency and voltage droop controllers, which is the existing approach.
- Case 2: Corresponds to the MG interfaces operating as VSGs with fixed inertia.
- Case 3: It is similar to Case 2 but with the proposed VSG adaptive inertia controllers.
- Case 4: Corresponds to Case 3 but with the proposed VFC and distributed system controllers.

Multiple sequential disturbances are simulated to test and compare the existing and proposed control approaches corresponding to the aforementioned study cases. Thus, first, the BESS and WG of ac MG 1 are disconnected at t=25 s, to simulate generation trip on an ac MG and its MMG system. This is followed by a 15% load shedding in ac MG 3 at t=35 s, to simulate load loss in an ac MG, as well as the MMG system. Then, a 50% reduction of solar PV power and a 25% reduction in BESS output power in dc MG 2 at t=50 s, to simulate generation loss in a dc MG and the associated MMG system. Finally, a three phase fault is applied at t=70 s at Bus 5 with a duration of 150 ms, to simulate a major fault in the system that results in MG and MMG instabilities.

The simulation results in Figure 11 depict the frequencies of the ac MGs for the aforementioned cases and disturbances. Note in Figure 11(a) that the MG 1 frequency successfully and rapidly recovers to its nominal value in Case 4 for the first disturbance, with Cases 3 and 4 showing better frequency response than the rest of the cases. Observe for the other cases that the frequency falls below its nominal value,

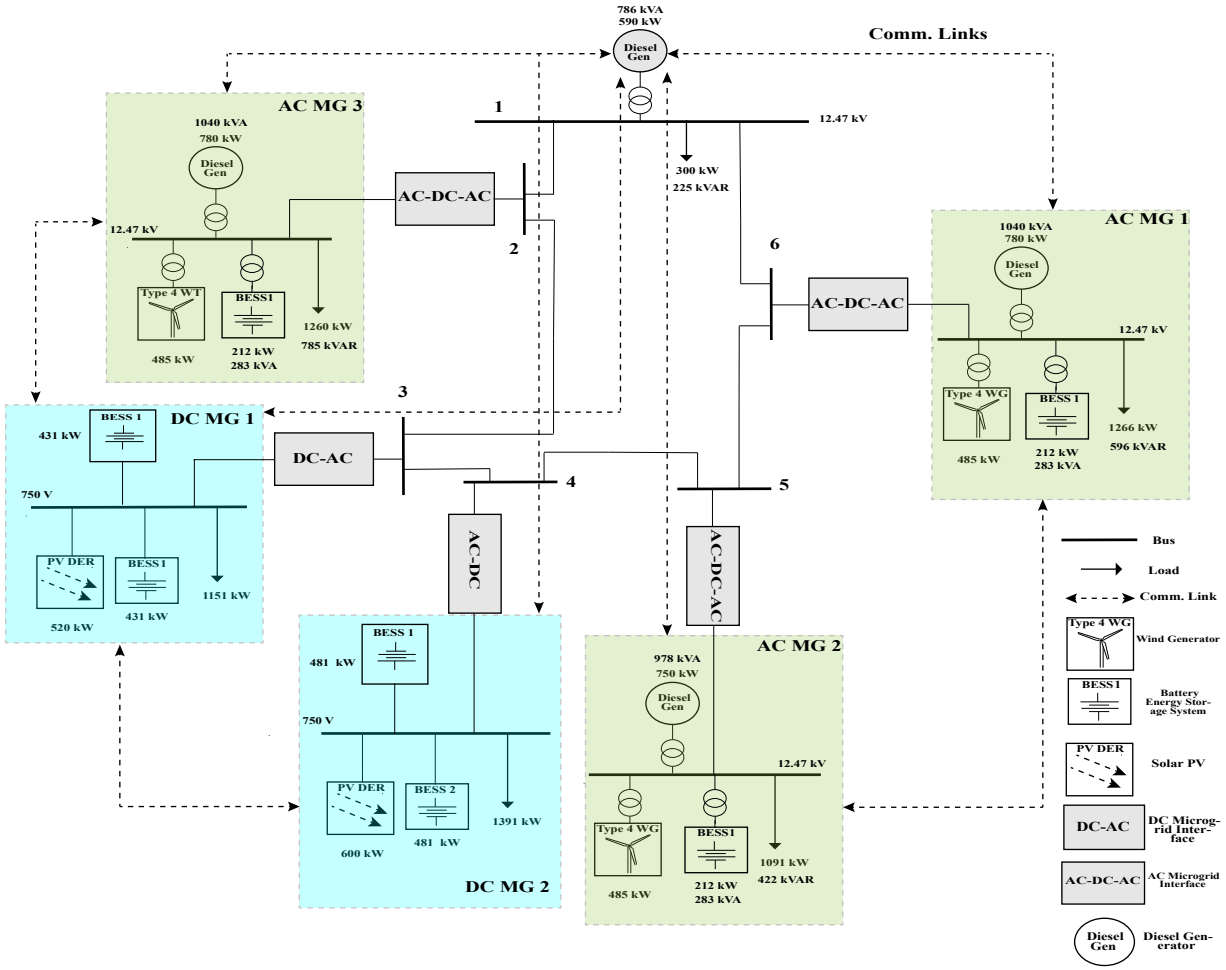
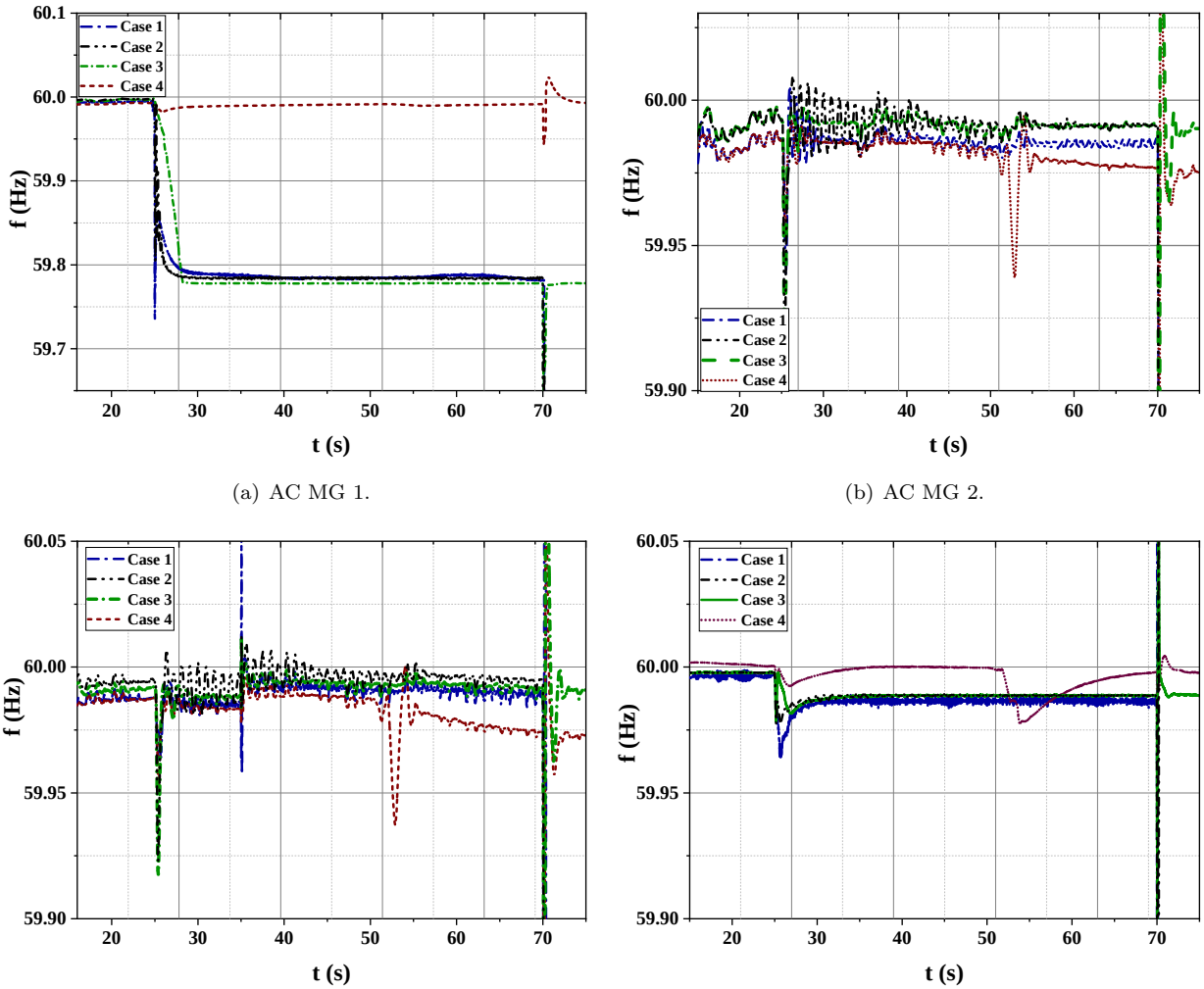


Figure 10: MMG test system derived from a CIGRE benchmark MG test system [30].

which could trigger system protections. Notice as well that the proposed controllers in Case 4 do not result in significant frequency deviations in the other ac MGs despite the increased power sharing, as shown in Figures 11(b) and 11(c); this is due to the VFC, which provides power reserves in the ac MGs by modulating the load voltages. Figure 11(c) shows the frequency of ac MG 3, with the sudden load interruption at 35 s resulting in an increase in the MG frequency for Cases 1, 2, and 3; however, in Case 4, the proposed distributed controller increases the power exchanged with the main grid at 50 s, since the exchanged power is a function of the frequency index defined in (31). Figures 12 and 13 illustrate the MMG system frequency deviations and associated statistics, respectively, where a superior performance can be observed with the proposed controllers that minimize the overall MMG frequency deviation.

Figure 14 shows the voltages of the dc MGs, where it can be seen that the disturbances result in dc voltage oscillations for Case 1 and 2. Note also in Figure 14(b) that the dc voltage of the dc MG 2 successfully recovers to its nominal value for Case 4, while for the other cases, the dc voltage deviates from its nominal value. It can also be observed that since the exchanged power of the MG with the main grid is dependent on the dc voltage index (31), the proposed distributed controller reduces its exchanged power with the rest of the system, since the disturbances result in a reduction of the dc voltage index for the MG. Finally, note that, in general, Case 4 shows better dc-voltage regulation and dynamic performance than the other cases. Figures 15 and 16 depict the MMG system dc-voltage deviations and associated statistics,



(a) AC MG 1.

(b) AC MG 2.

(c) AC MG 3.

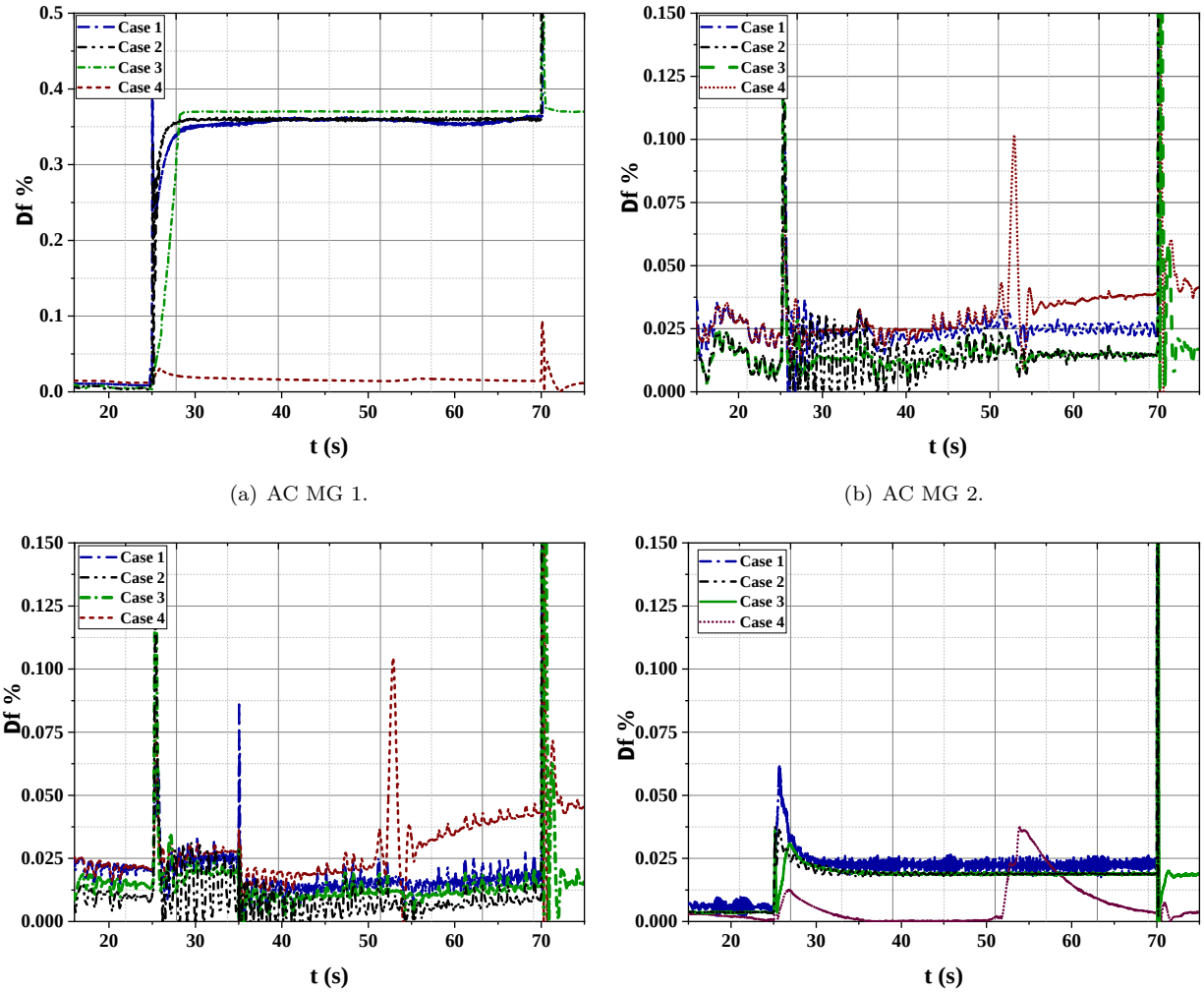
(d) Host grid.

Figure 11: MMG system frequencies for the different disturbances.

respectively, demonstrating a superior performance with the proposed controllers which minimize the overall MMG dc-voltage deviations.

Observe in Figures 11 and 14 that the Bus 5 three-phase fault at t=70 s results in instabilities for Cases 1 and 2. However, for Case 3 and 4, the system recovers and is stable due to the proposed adaptive inertia.

Figures 17 to 20 illustrate the performance of the overall MMG system for all the proposed controllers in Case 4, which results in the best overall system performance and stability. Thus, Figure 17 depicts the interfacing VSGs' active output powers with the proposed coordination technique. Figure 18 illustrates the impact of the VFC on the voltages of the ac MGs and the host grid. Finally, Figures 19 and 20 show the changes in the moment of inertia and the damping coefficient of the VSG interfaces due to the proposed adaptive inertia controller, illustrating the expected variations on these controller parameters as the MMG system condition change.



(a) AC MG 1.

(b) AC MG 2.

(c) AC MG 3.

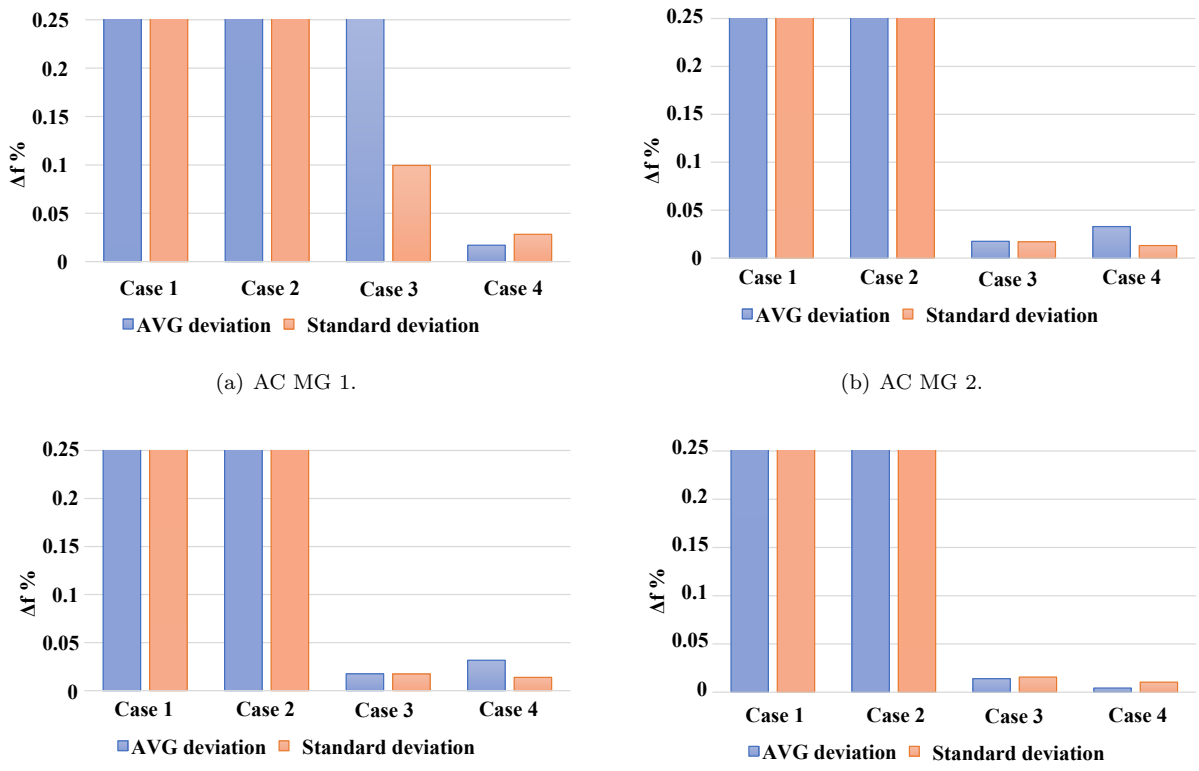
(d) Host grid.

Figure 12: AC MMG system frequency deviations for the different disturbances.

5. Conclusion

A hierarchical distributed control system was proposed and developed to regulate the frequencies and voltages of an ac/dc multi-microgrid system. The controller was integrated into a network architecture based on interfacing the microgrids with virtual-synchronous-generator-based microgrid interfaces, which offers the following advantages over existing control techniques:

- The proposed interface provides virtual inertia through the realization of the synchronous generator swing equation, enhancing frequency and voltage regulation for a multi-microgrid system.
- The presented new control technique improves the system's frequency and dc voltage responses by adjusting the inertia and damping constants of the interfacing virtual synchronous generators, minimizing power oscillations in both ac and dc microgrids, and limiting frequency and voltage excursions.
- The proposed distributed controller, based on an adaptive consensus technique, coordinates the output power of both ac and dc microgrids to regulate the frequencies and the dc voltages of all microgrids based on local microgrid measurements.



(a) AC MG 1.

(b) AC MG 2.

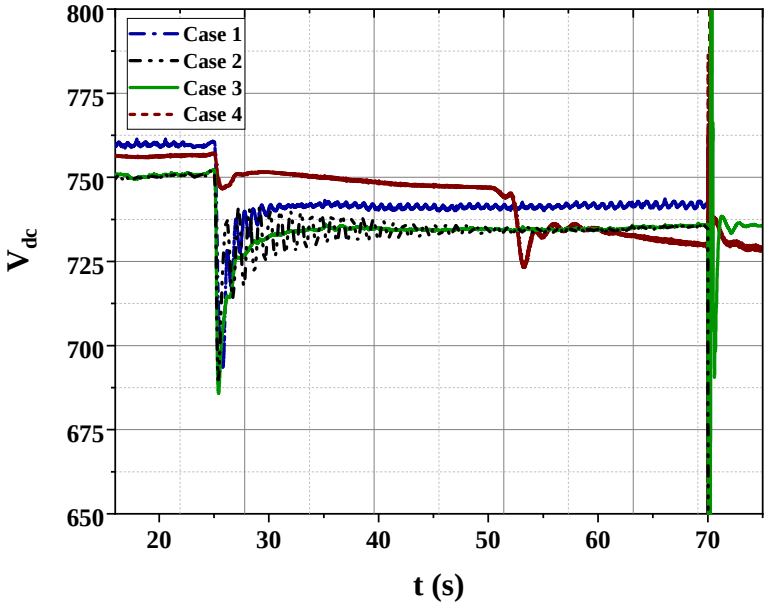
(c) AC MG 3.

(d) Host grid.

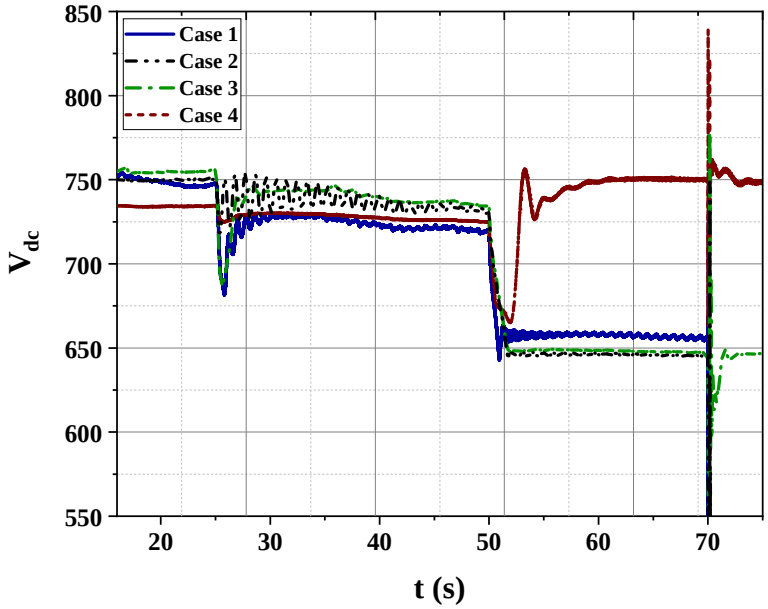
Figure 13: AC MMG system frequency deviation statistics extracted from Figure 12.

- The discussed control schemes can be readily scaled up for larger multi-microgrid systems, with minimum communication bandwidth and infrastructure, which is an issue with existing centralized controllers that are prone to single point failures.
- The results obtained for a test ac/dc multi-microgrid demonstrate that the proposed virtual-synchronous-generator-based adaptive inertia and damping controllers for the microgrid interfaces, properly coordinated by the proposed distributed control approach, outperform existing control techniques.

Future study direction may include the development of a detailed linearized mathematical model of the virtual synchronous generator interfaces for eigenvalue analyses, so that the impact of these interfaces on multi-microgrid systems can be studied in more detail.

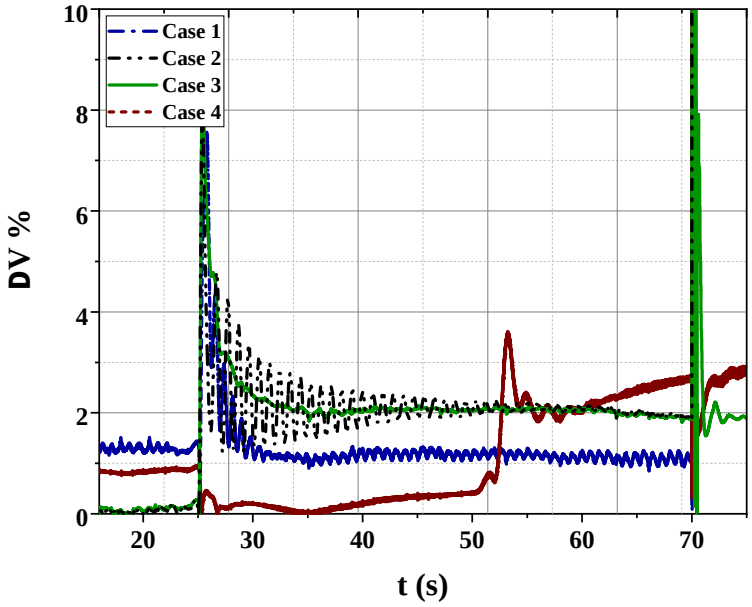


(a) DC MG 1.

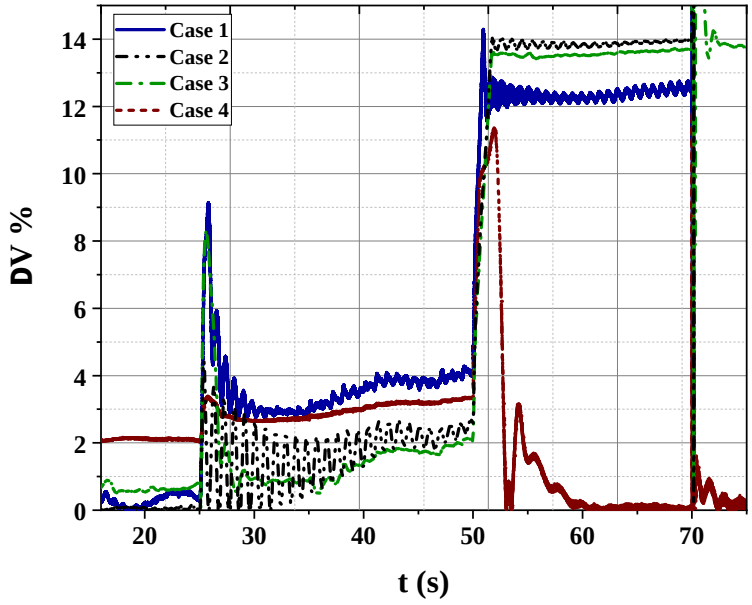


(b) DC MG 2.

Figure 14: DC MG voltages for the different disturbances.

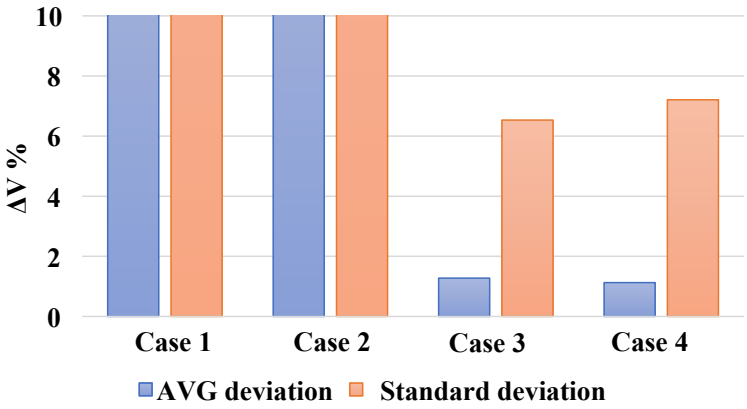


(a) DC MG 1.

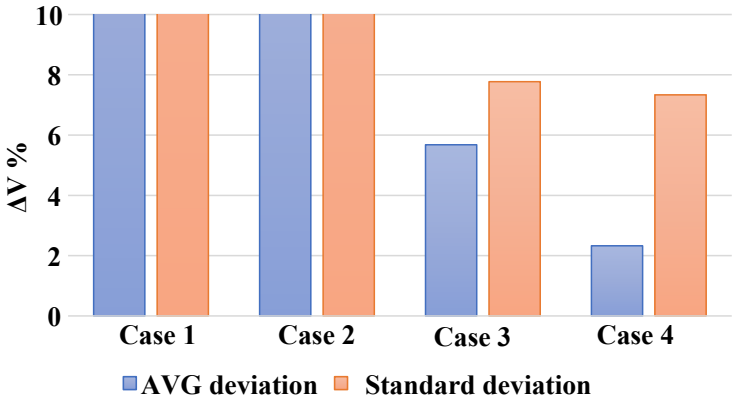


(b) DC MG 2.

Figure 15: DC MG voltage deviations for the different disturbances.



(a) DC MG 1.



(b) DC MG 2.

Figure 16: DC MG voltage deviation statistics extracted from Figure 15.

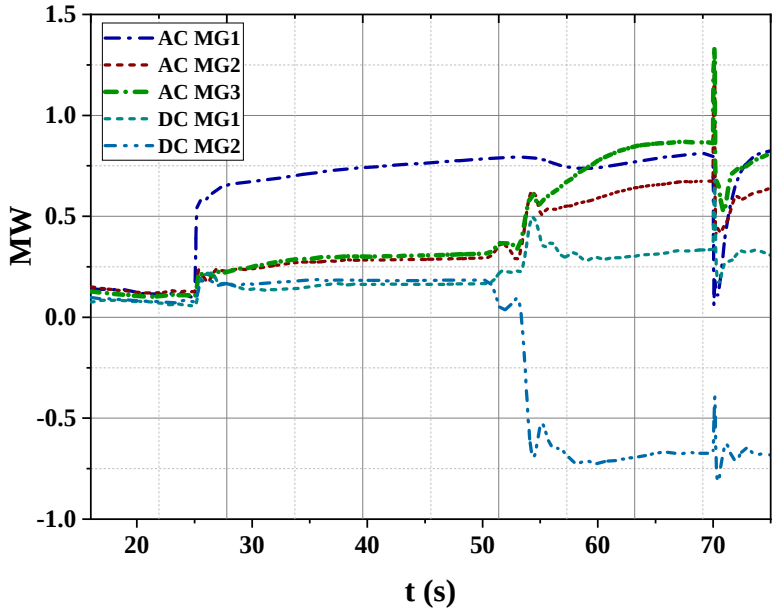


Figure 17: Output powers of the VSG interfaces for Case 4.

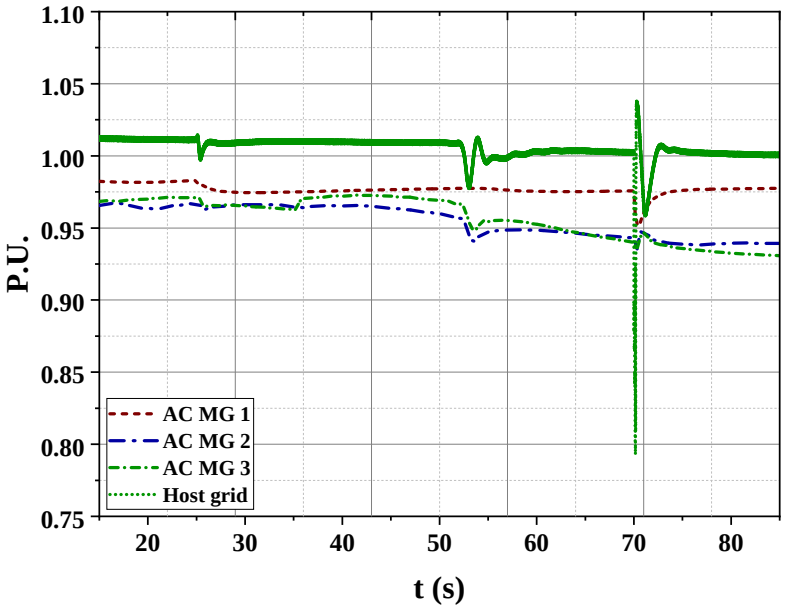


Figure 18: Voltages of the ac MGs and host grid for Case 4.

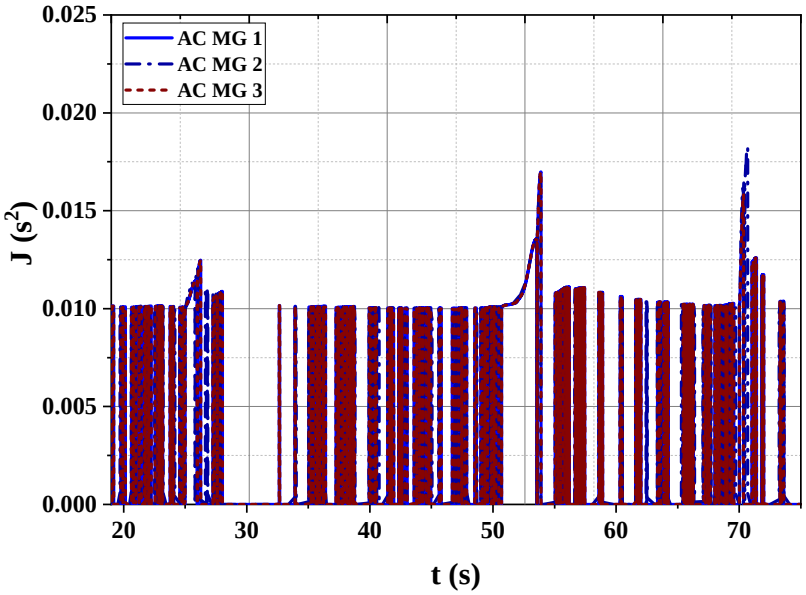


Figure 19: Inertia of B2B VSG interfaces for Case 4.

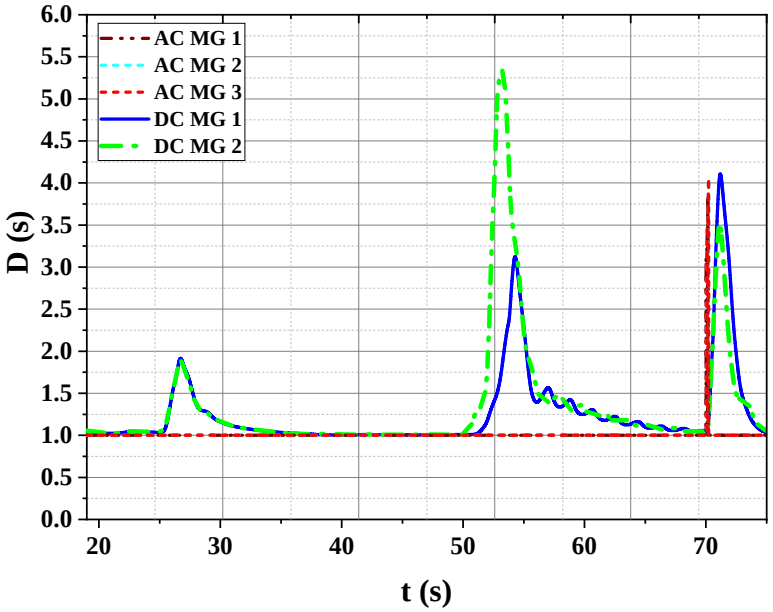


Figure 20: Damping coefficient of all dc-ac VSG interfaces for Case 4.

References

[1] M. S. Mahmoud (Ed.), Microgrid: Advanced Control Methods and Renewable Energy System Integration, 1st Edition, Butterworth-Heinemann, 2016.

[2] E. Bullich-Massagué, F. Díaz-González, M. Aragüés-Peñalba, F. Girbau-Llistuella, P. Olivella-Rosell *et al.*, Microgrid clustering architectures, Applied Energy 212 (2018) 340–361.

[3] IEEE standard for interconnection and interoperability of distributed energy resources with associated electric power systems interfaces, IEEE Std 1547-2018 (Revision of IEEE Std 1547-2003) (2018).

[4] A. Ouammi, H. Dagdougui, L. Dessaint, R. Sacile, Coordinated model predictive-based power flows control in a cooperative network of smart microgrids, IEEE Transactions on Smart Grid 6 (5) (2015) 2233–2244.

[5] H. Dagdougui, A. Ouammi, R. Sacile, Optimal control of a network of power microgrids using the Pontryagin's minimum principle, IEEE Transactions on Control Systems Technology 22 (5) (2014) 1942–1948.

[6] V. Toro, E. Mojica-Nava, Droop-free control for networked microgrids, in: 2016 IEEE Conference on Control Applications (CCA), 2016, pp. 374–379.

[7] N. Gil, J. Abel, Exploiting automated demand response, generation and storage capabilities for hierarchical frequency control in islanded multi-microgrids, in: PSCC, 2008, p. 1–7.

[8] A. Ghafouri, J. Milimonfared, G. B. Gharehpetian, Coordinated control of distributed energy resources and conventional power plants for frequency control of power systems, IEEE Transactions on Smart Grid 6 (1) (2015) 104–114.

[9] S. Moayedi, A. Davoudi, Distributed tertiary control of dc microgrid clusters, IEEE Transactions on Power Electronics 31 (2) (2016) 1717–1733.

[10] Z. Wang, F. Liu, Y. Chen, S. H. Low, S. Mei, Unified distributed control of stand-alone dc microgrids, IEEE Transactions on Smart Grid 10 (1) (2019) 1013–1024.

[11] J. Mírez, A modeling and simulation of optimized interconnection between dc microgrids with novel strategies of voltage, power and control, in: 2017 IEEE Second International Conference on DC Microgrids (ICDCM), 2017, pp. 536–541.

[12] M. Hamzeh, M. Ghafouri, H. Karimi, K. Sheshyekani, J. M. Guerrero, Power oscillations damping in dc microgrids, IEEE Transactions on Energy Conversion 31 (3) (2016) 970–980.

[13] X. Chang, Y. Li, X. Li, X. Chen, An active damping method based on a supercapacitor energy storage system to overcome the destabilizing effect of instantaneous constant power loads in dc microgrids, IEEE Trans. Energy Conversion 32 (1) (2017) 36–47.

[14] P. Wu, W. Huang, N. Tai, S. Liang, A novel design of architecture and control for multiple microgrids with hybrid ac/dc connection, Applied Energy 210 (2018) 1002–1016.

[15] X. Zhou, L. Zhou, Y. Chen, J. M. Guerrero, A. Luo, W. Wu *et al.*, A microgrid cluster structure and its autonomous coordination control strategy, International Journal of Electrical Power & Energy Systems 100 (2018) 69–80.

[16] H. Bevrani, T. Ise, Y. Miura, Virtual synchronous generators: A survey and new perspectives, International Journal of Electrical Power & Energy Systems 54 (2014) 244–254.

[17] S. D'Arco, J. A. Suul, O. B. Fosso, Small-signal modelling and parametric sensitivity of a virtual synchronous machine, in: PSCC, 2014, pp. 1–9.

[18] S. D'Arco, J. A. Suul, O. B. Fosso, A virtual synchronous machine implementation for distributed control of power converters in smartgrids, Electric Power Systems Research 122 (2015) 180–197.

[19] A. Yazdani, Voltage-sourced Converters in Power Systems: Modeling, Control, and Applications, IEEE Press/John Wiley, Hoboken, N.J, 2010.

[20] M. Farrokhabadi, C. A. Cañizares, J. W. Simpson-Porco, E. Nasr, L. Fan, P. A. Mendoza-Araya *et al.*, Microgrid stability definitions, analysis, and examples, IEEE Transactions on Power Systems 35 (1) (2020) 13–29.

[21] M. Farrokhabadi, S. König, C. A. Cañizares, K. Bhattacharya, T. Leibfried, Battery energy storage system models for microgrid stability analysis and dynamic simulation, IEEE Transactions on Power Systems 33 (2) (2018) 2301–2312.

[22] R. Teodorescu, Grid Converters for Photovoltaic and Wind Power Systems, IEEE Wiley, Piscataway, New Jersey Chichester, West Sussex, 2011.

[23] M. Farrokhabadi, C. A. Cañizares, K. Bhattacharya, Frequency control in isolated/islanded microgrids through voltage regulation, IEEE Transactions on Smart Grid 8 (3) (2017) 1185–1194.

[24] J. Alipoor, Study on stabilization of power system with distributed generations using virtual synchronous generator, Ph.D. thesis, Osaka University (2015).

[25] V. Nasirian, Q. Shafiee, J. M. Guerrero, F. L. Lewis, A. Davoudi, Droop-free distributed control for ac microgrids, IEEE Transactions on Power Electronics 31 (2) (2016) 1600–1617.

[26] IEC 60038 standard voltages, defines a set of standard voltages for use in low voltage and high voltage AC and DC electricity supply systems. , IEC 60038 std voltages (2009) 1–26.

[27] M. Farrokhabadi, C. Cañizares, K. Bhattacharya, A voltage-based frequency controller for inverter-based systems in microgrids, in: 2016 IEEE Power and Energy Society General Meeting (PESGM), 2016, pp. 1–5.

[28] X. Wang, P. Wilson, D. Woodford, Interfacing transient stability program to EMTDC program, in: Proceedings. International Conference on Power System Technology, Vol. 2, 2002, pp. 1264–1269.

[29] B. Alghamdi, K. Wieninger, C. A. Cañizares, Distributed voltage control of dc microgrids, in: 2020 AEIT International Annual Conference, 2020, pp. 1–6.

[30] B. Alghamdi, Frequency and Voltage Control of a Grid of Microgrids, Ph.D. thesis, University of Waterloo, ON, Canada (2021).